# ENERGY HARVESTING BY EXPLOITING VORTEX-INDUCED VIBRATION FROM A MODIFIED CRUCIFORM STRUCTURE

AHMAD ADZLAN FADZLI BIN KHAIRI

UNIVERSITI TEKNOLOGI MALAYSIA

# ENERGY HARVESTING BY EXPLOITING VORTEX-INDUCED VIBRATION FROM A MODIFIED CRUCIFORM STRUCTURE

AHMAD ADZLAN FADZLI BIN KHAIRI

A thesis submitted in fulfilment of the
requirements for the award of the degree of
Doctor of Philosophy

Malaysia-Japan International Institute of Technology
Universiti Teknologi Malaysia

JUNE 2022

## DEDICATION

My dearest wife and children. Respected supervisor and colleagues at the WEE iKohza. This is for all of you.

## ACKNOWLEDGEMENT

I would like to first express my highest sense of gratitude to my supervisor Assoc. Prof Dr Mohamed Sukri Mat Ali. His knowledge and proficiency in computational fluid dynamics have made my entry into this field of study a little bit more bearable and has since been an excellent tool in making novel discoveries and conclusions. His open stance in receiving ideas and suggestions to strengthen the foundations of this research has been fundamental to the preservation of the originality and timeliness of this work. I have learned a lot from him about the value of logical continuity and how to achieve it throughout the course of completing this work. The relentless effort for logical continuity throughout the thesis has been, in my opinion, crucial towards a manuscript that not only is easily accessible but helps target audiences to build upon this work in the future, hence advancing the field as a whole.

As for my beloved family, especially my wife and two babies, I really cannot think of any way to repay your hardships and understanding throughout the years of my study. Even a lifetime of unconditional love and devotion towards all of you squares only but a small fraction of what you have given up making my studies a reality. To that end I can only trust the Most Merciful to fully even the debt and make all of you among those who are most beloved by the Most Gracious. I pray to the Almighty to accept the fruit of our jihad in finding knowledge and may all the trials and tribulations we have encountered together, physically, psychologically and financially, will stand witness in the hereafter that we have answered His call towards submission, and His call towards success. Aamin ya Rabbal ‘alamin.

## ABSTRACT

From off-grid charging of electronic devices to energising independent wireless sensor networks, the demand for stand-alone, low-power generators from renewable energy sources is becoming more prevalent. A cruciform energy harvester has been shown to output consistent power in the order of 1 mW when the reduced velocity $U^*$, exceeds 15. However, this output is insufficient and its onset too late for real-world applications. Thus, this study seeks to remedy these two shortcomings by investigating cruciforms oscillators at various cruciform angles. To fulfill these goals, the Reynolds-Averaged Navier-Stokes simulation were performed, and the results for the 90° cruciform were compared against experimental data for validation. The experiment uses a similar 90° cruciform in an open flow channel. Assessments were made on the vibration amplitude, frequency, lift amplitude and lift frequency at cruciform angles 90°, 67.5°, 45°, 22.5° and 0°. The Reynolds number range was $1.1\times10^3 \leq \mathrm{Re} \leq 14.6\times10^3$ and Scruton number 9.94, which was consistent with similar studies. Hilbert-Huang analysis of the 90° cruciform indicated that a lot of energy from the free stream was wasted in the production of non-performing Karman vortices. A larger lift was possible if streamwise vortices were produced instead. When $45 \leq \alpha(^\circ) \leq 67.5$, asymmetries in the vortical structures prevented high-amplitude vibrations from taking place. However, when $0 \leq \alpha(^\circ) \leq 22.5$, a high-degree of symmetry among the vortical structures led to an early onset of high-amplitude vibration. Power generated by the cruciform was in the order of 1 mW for a 90° cruciform, below 1 mW when $45 \leq \alpha(^\circ) \leq 67.5$, and in the order of 10 mW when $0 \leq \alpha(^\circ) \leq 22.5$. Unification of the power generation and energy harvesting efficiency results produced a map that describes the power and efficiency of the harvester in the $\alpha(^\circ) - U^*$ parameter space. This uncovers three distinct regions of power generation: pure cruciform region as cruciform angle tends to 90°, steep-angle region between $45 \leq \alpha(^\circ) \leq 67.5$, and shallow-angle region between $0 \leq \alpha(^\circ) \leq 22.5$. Maximum efficiency occurs close to 0.8 m/s when cruciform angle is 90°, close to 0.2 m/s at 67.5°, and close to 0.4 m/s at 0°. This power and efficiency map makes it possible for future engineers to tailor the design of their cruciform energy harvester to their specific power and efficiency needs.

## ABSTRAK

Daripada pengecasan peranti elektronik di luar grid sehingga pentenagaan rangkaian sensor tanpa wayar, permintaan untuk sistem janakuasa berskala kecil dari sumber tenaga boleh diperbaharui adalah semakin meningkat. Sebuah pemungut tenaga krusiform menghasilkan kuasa sekitar 1mW apabila halaju terturun $U^*$ lebih besar daripada 15. Walau bagaimanapun, output ini tidak mencukupi dan permulaannya terlalu lewat untuk aplikasi dunia sebenar. Kajian ini bertujuan untuk mengatasi dua masalah tersebut dengan menyelidik pengayun krusiform pada sudut krusiform yang pelbagai. Simulasi Navier-Stokes Purata-Reynolds telah dijalankan, dan data dari krusiform 90° telah dibandingkan dengan data eksperimen untuk pengesahan. Eksperimen tersebut juga menggunakan krusiform 90° dalam sebuah kanal aliran terbuka. Penilaian dijalankan terhadap amplitude getaran, frekuensi, serta amplitud dan frekuensi daya angkat pada sudut krusiform 90°, 67.5°, 45°, 22.5° dan 0°. Nombor Reynolds adalah $1.1 \times 10^3 \leq \mathrm{Re} \leq 14.6 \times 10^3$, manakala nombor Scruton adalah 9.94. Analisis Hilbert-Huang pada sudut 90° menunjukkan terdapat banyak tenaga yang terbazir dalam menghasilkan vortex Karman. Daya angkat yang lebih besar boleh diperoleh sekiranya vorteks arus yang dihasilkan. Pada sudut $45 \leq \alpha\ (^\circ) \leq 67.5$, asimetri pada struktur vortex menghalang penjanaan amplitud getaran yang tinggi. Walau bagaimanapun, apabila $0 \leq \alpha\ (^\circ) \leq 22.5$, simetri yang tinggi pada struktur vorteks menyebabkan getaran amplitud tinggi bermula lebih awal. Penyatuan data output kuasa dan kecekapan menghasilkan peta output kuasa dan kecekapan dalam ruang parameter $\alpha\ (^\circ) - U^*$. Ini membawa kepada penemuan tiga rantau penjanaan kuasa: rantau krusiform asli apabila sudut krusiform menghampiri 90°, krusiform curam apabila $45 \leq \alpha\ (^\circ) \leq 67.5$, dan krusiform cetek apabila $0 \leq \alpha\ ^\circ \leq 22.5$. Kecekapan maksimum terhasil sekitar 0.8 m/s dan sudut krusiform 90°, sekitar 0.2 m/s pada 67.5° dan sekitar 0.4 m/s pada 0°. Peta kuasa dan kecekapan ini membolehkan jurutera masa hadapan mengubahsuai pemungut tenaga krusiform mereka mengikut keperluan kuasa dan kecekapan yang diperlukan.

## TABLE OF CONTENTS


| | TITLE | PAGE |
|---|---|---|
| | **DECLARATION** | **ii** |
| | **DEDICATION** | **iii** |
| | **ACKNOWLEDGEMENT** | **iv** |
| | **ABSTRACT** | **v** |
| | **ABSTRAK** | **vi** |
| | **TABLE OF CONTENTS** | **vii** |
| | **LIST OF TABLES** | **x** |
| | **LIST OF FIGURES** | **xi** |
| | **LIST OF ABBREVIATIONS** | **xvii** |
| | **LIST OF SYMBOLS** | **xix** |
| | **LIST OF APPENDICES** | **xxi** |
| **CHAPTER 1** | **INTRODUCTION** | **1** |
| | 1.1 Background of Study | 1 |
| | 1.2 Problem Statement | 7 |
| | 1.3 Research Questions | 8 |
| | 1.4 Thesis Objectives | 9 |
| | 1.5 Scope of Works | 10 |
| | 1.6 Significance of Study | 12 |
| | 1.7 Thesis Organisation | 13 |
| **CHAPTER 2** | **LITERATURE REVIEW** | **16** |
| | 2.1 Vortex Shedding from a Cylinder | 16 |
| | 2.1.1 Karman Vortex Shedding | 17 |
| | 2.1.2 Streamwise Vortex Shedding | 22 |
| | 2.2 Vortex-induced Vibration of a Cylinder | 32 |
| | 2.2.1 Single Cylinder Oscillator Unit | 32 |
| | 2.2.2 Cruciform Oscillator Unit | 36 |
| | 2.3 Energy Harvesting from a Vibrating Cylinder | 41 |
| | 2.3.1 Single Cylinder System | 41 |

2.3.2 Pure Cruciform System 45
2.4 Methodologies in VIV Studies 49
2.4.1 Vibration Parameters 49
2.4.2 Solution of Governing Equations 52
2.4.3 Dynamic Mesh Motion 53
2.4.4 Ensemble Empirical Mode Decomposition and Hilbert Transform 57
2.5 Chapter Summary 59

**CHAPTER 3 METHODOLOGY 63**
3.1 Design Geometry 65
3.2 Numerical Solution 71
3.3 Open Flow Channel Experiment 72
3.4 Phase Lag Between $C_L$ and Normalised Cylinder Displacement 76
3.5 Estimation of Power 76
3.6 Grid Independency Study 78
3.7 Chapter Summary 80

**CHAPTER 4 RESULTS AND DISCUSSION 82**
4.1 Experimental Apparatus Benchmarking 82
4.2 The Grid Convergence Index Study 83
4.3 The Pure Cruciform 86
4.3.1 The Amplitude and Frequency Response 86
4.3.2 Main Vibration-driving Vortical Structure 93
4.3.3 Temporal Evolution of the Lift Coefficient 96
4.3.3.1 The KVIV Regime (Reduced Velocity Below 13.6) 97

4.3.3.2 Transition to SVIV (Reduced Velocity Between 15.9 and 18.2) 102
4.3.3.3 The Stable SVIV Regime (Reduced Velocity Greater Than 20.5) 107
4.3.4 Harnessable Power 109
4.3.5 Possibility for Increasing Fluid Power 111
4.4 Steep-angled Cruciforms 114
4.4.1 The Amplitude and Frequency Response 115
4.4.2 Main Vibration-driving Vortical Structure 118
4.4.3 Phase Lag Between $C_L$ and Normalised Cylinder Displacement 124
4.5 Shallow-angled Cruciforms 125
4.5.1 The Amplitude and Frequency Response 126
4.5.2 Main Vibration-driving Vortical Structure 129
4.5.3 Phase Lag Between $C_L$ and Normalised Cylinder Displacement 136
4.6 Power Characteristic in Cruciform Angle - Reduced Velocity Parameter Space 138
4.7 Chapter Summary 141

**CHAPTER 5 CONCLUSION 144**
5.1 Recommendation of Future Works 146

**REFERENCES 147**
**LIST OF PUBLICATIONS 163**

## LIST OF TABLES


| TABLE NO. | TITLE | PAGE |
|---|---|---|
| Table 2.1 | Empirical constants used in the Spalart-Allmaras turbulence model. | 53 |
| Table 2.2 | Summary of findings in literature and key takeaways. | 61 |
| Table 3.1 | Values of parameters investigated in previous studies. | 66 |
| Table 3.2 | The list of conditions investigated in this study. | 71 |
| Table 3.3 | The specifications of the HP Z420 workstation | 72 |
| Table 3.4 | Summary of experimental parameters in contrast to those used in the experimental work of Koide *et al.* (2013). | 73 |
| Table 4.1 | Summary of grid independency study. | 84 |
| Table 4.2 | Summary of main findings. | 138 |

## LIST OF FIGURES


| FIGURE NO. | TITLE | PAGE |
|---|---|---|
| Figure 1.1 | Number of publications with keywords ["vortex induced vibration" energy]. Retrieved from SCOPUS. | 3 |
| Figure 1.2 | Apparent power $P_a$ (W) versus reduced velocity $U^*$ for cases of KVIV and SVIV. Adapted from Koide *et al.* (2013). | 6 |
| Figure 2.1 | Evolution of Karman vortex shedding from a two-dimensional circular cylinder at increasing Reynolds number. | 18 |
| Figure 2.2 | Force coefficients versus Re summarised by Zdravkovich (1997). | 19 |
| Figure 2.3 | Stretching of the vortex line on a Karman vortex creates streamwise vorticity. Adapted from Williamson (1996b). | 23 |
| Figure 2.4 | Three-dimensional visualisation of mode A of Karman vortex shedding. Adapted from Thompson *et al.* (1994). | 24 |
| Figure 2.5 | Three-dimensional visualisation of mode B of Karman vortex shedding. Adapted from Thompson *et al.* (1994). | 24 |
| Figure 2.6 | The conical shroud used by Lin *et al.* (2018). | 27 |
| Figure 2.7 | Some examples of the Ω-vortices from Lin *et al.* (2018), taken at different times of the simulation. | 28 |
| Figure 2.8 | A schematic of streamwise vortex shedding, adapted from Hemsuwan *et al.* (2018a). | 30 |
| Figure 2.9 | The two-circular cylinder system of Ding *et al.* (2017). | 35 |
| Figure 2.10 | The two-circular cylinder cruciform of Zhao and Lu (2018). | 37 |
| Figure 2.11 | Schematic of the base configuration of the oscillator system used in this study, i.e. the pure cruciform. | 39 |
| Figure 2.12 | A three-dimensional drawing of the system to control the mechanical parameters of the system. Adapted from Ma *et al.* (2018). | 42 |
| Figure 2.13 | The vibration-to-electrical energy converter of Koide *et al.* (2009). | 46 |

| | | |
|---|---|---|
| Figure 2.14 | Steady lift production from streamwise vortex. Adapted from Hemsuwan *et al.* (2021). | 48 |
| Figure 2.15 | The free-body diagram of Maruai (2019). | 49 |
| Figure 2.16 | The free-body diagram of the cruciform oscillator. | 50 |
| Figure 2.17 | Free-vibration response of the vibrating system. | 50 |
| Figure 2.18 | An example application of ACMI between two differently meshed regions. Adapted from Yang *et al.* (2022). | 56 |
| Figure 2.19 | The pyramid of knowledge for the cruciform energy harvester. | 60 |
| Figure 3.1 | The first part of the methodology. This includes the pilot data collection, validation of numerical model and main data collection. | 63 |
| Figure 3.2 | The second part of the methodology. This covers the data analysis part of the study. | 64 |
| Figure 3.3 | Schematic of the computational domain. | 67 |
| Figure 3.4 | The three-dimensional domain, side view. | 68 |
| Figure 3.5 | The three-dimensional domain, top view. | 68 |
| Figure 3.6 | Cruciform layout for 90°. | 69 |
| Figure 3.7 | Cruciform layout for 67.5°. | 69 |
| Figure 3.8 | Cruciform layout for 45°. | 70 |
| Figure 3.9 | Cruciform layout for 22.5°. | 70 |
| Figure 3.10 | Cruciform layout for 0°. | 70 |
| Figure 3.11 | The experimental apparatus used to validate the pilot numerical results. | 73 |
| Figure 3.12 | Sketch of the experimental system used in this study. | 74 |
| Figure 3.13 | Close-up of the magnetic damper. | 75 |
| Figure 3.14 | The course, medium and fine mesh used in the grid independency study. | 78 |
| Figure 4.1 | Experimentally measured $y^*(t)$, which is the normalised cylinder displacement time series. | 83 |
| Figure 4.2 | Richardson extrapolation of $y^*_{\mathrm{RMS}}$, $f^*$ and $\mathrm{C_{L,RMS}}$. | 85 |
| Figure 4.3 | The error between the values of $y^*$, $f^*$ and $\mathrm{C_{L,RMS}}$ and their corresponding Richardson extrapolation. | 86 |

Figure 4.4 Evolution of the normalised root-mean-square amplitude of cylinder displacement $y^*_{\mathrm{RMS}}$, with respect to reduced velocity $U^*$, in the streamwise vortex-driven vibration regime. 87
Figure 4.5 Comparison between the evolution of $y^*_{\mathrm{RMS}}$ with respect to $U^*$ of a pure cruciform system from the numerical and experimental work. The filled square represents the numerical, while the filled circle represents the experimental results. 88
Figure 4.6 Evolution of the normalised cylinder displacement frequency, $f^*$, with respect to reduced velocity $U^*$, for the pure cruciform case. 90
Figure 4.7 Comparison between the numerical and experimental data of $f^*$ for the pure cruciform. 91
Figure 4.8 Evolution of the lift coefficient root-mean-square amplitude ($\mathrm{C_{L,RMS}}$) and normalised frequency of lift coefficient ($f^*_{\mathrm{C}_l}$), with respect to reduced velocity $U^*$, for the pure cruciform case. The dashed line in Fig. 4.8b visualises the shedding frequency of Karman vortex computed from Eq. 2.6. 92
Figure 4.9 Distribution of normalised frequency of vortex shedding, along the span of the cylinder of the pure cruciform at $U^* = 22.7$. 94
Figure 4.10 Dominant vortical structures at $U^* = 22.7$ observed in the pure cruciform case. 94
Figure 4.11 The Q-criterion for the 90° cruciform at $U^* = 22.7$: the isometric (4.11a) and plan view (4.11b). 96
Figure 4.12 The Q-criterion for the 90° cruciform at $U^* = 6.8$: the isometric (4.12a) and plan view (4.12b). 96
Figure 4.13 Temporal analysis of $\mathrm{C_L}$ and $y^*$ at $U^* = 4.5$. 98
Figure 4.14 Temporal analysis of $\mathrm{C_L}$ and $y^*$ at $U^* = 6.8$. 99
Figure 4.15 Temporal analysis of $\mathrm{C_L}$ and $y^*$ at $U^* = 13.6$. 101
Figure 4.16 Temporal evolution of $y^*$ and $\mathrm{C_L}$ at $U^* = 15.9$. 103
Figure 4.17 Temporal analysis of the $\mathrm{C_L}$ and $y^*$ signal at $U^* = 15.9$. 104

Figure 4.18 Temporal analysis of the lift coefficient and normalised cylinder displacement signal at $U^* = 18.2$. 106
Figure 4.19 The instantaneous phase lag $\phi$ of $C_{C_L,y^*}$ in the range $20.5 \leq U^* \leq 29.5$. 108
Figure 4.20 Variation of $\theta_{y-\mathrm{Cl}}$ with respect to $U^*$ for the pure cruciform. 109
Figure 4.21 Estimation of $P_{\mathrm{Mech.,RMS}}$ and $P_{\mathrm{Fluid,RMS}}$ and comparison with available data. 110
Figure 4.22 The HHT spectrogram of $\mathrm{C_L}$ between $20.5 \leq U^* \leq 29.5$. The solid and dashed line white boxes dilineate the distribution of the streamwise and Karman components of lift, respectively. 112
Figure 4.23 Evolution of $C_{F_L,\mathrm{Karman,RMS}}$ and $C_{F_L,\mathrm{streamwise,RMS}}$ with respect to $U^*$. 113
Figure 4.24 Evolution of the normalised vibration amplitude $y^*_{\mathrm{RMS}}$, with respect to reduced velocity $U^*$, for the 67.5° and 45° cruciforms. 115
Figure 4.25 Evolution of the normalised cylinder displacement frequency, $f^*$, with respect to reduced velocity $U^*$, for the 67.5° and 45° cruciforms. 116
Figure 4.26 Evolution of the normalised $\mathrm{C_L}$ root-mean-square amplitude, $\mathrm{C_{L,RMS}}$, with respect to reduced velocity $U^*$, for the 67.5° and 45° cruciforms. 117
Figure 4.27 Evolution of the normalised $\mathrm{C_L}$ frequency, $f^*_{\mathrm{C}_l}$, with respect to reduced velocity $U^*$, for the 67.5° and 45° cruciforms. The dashed lines outline $f_{v,\mathrm{Karman}}$ from Eq. 2.6. 118
Figure 4.28 Distribution of normalised frequency of vortex shedding, along the span of the cylinder of the 67.5° and 45° cruciforms at $U^* = 22.7$. 119
Figure 4.29 Dominant vortical structures at $U^* = 22.7$ observed in the 67.5° and 45° cases. 120
Figure 4.30 The Q-criterion for the 67.5° cruciform at $U^* = 4.5$: the isometric (4.30a) and plan view (4.30b). 122
Figure 4.31 The Q-criterion for the 67.5° cruciform at $U^* = 22.7$: the isometric (4.31a) and plan view (4.31b). 122

Figure 4.32 The Q-criterion for the 45° cruciform at $U^*$ = 4.5: the isometric (4.32a) and plan view (4.32b). 123
Figure 4.33 The Q-criterion for the 45° cruciform at $U^*$ = 22.7: the isometric (4.33a) and plan view (4.33b). 123
Figure 4.34 Phase lag $\theta_{y-C_L}$ (°) between $C_L$ and $y^*$ when 67.5° and 45°. 125
Figure 4.35 Evolution of the normalised vibration amplitude $y^*_{RMS}$, with respect to reduced velocity $U^*$, for the 22.5° and 0° cruciforms. 126
Figure 4.36 Evolution of the normalised cylinder displacement frequency, $f^*$, with respect to reduced velocity $U^*$, for the 22.5° and 0° cruciforms. 127
Figure 4.37 Evolution of the normalised $C_L$ root-mean-square amplitude, $C_{L,RMS}$, with respect to reduced velocity $U^*$, for the 22.5° and 0° cruciforms. 128
Figure 4.38 Evolution of the normalised $C_L$ frequency, $f^*_{C_l}$, with respect to reduced velocity $U^*$, for the 22.5° and 0° cruciforms. The dashed lines outline $f_{v,Karman}$ from Eq. 2.6. 128
Figure 4.39 Distribution of normalised frequency of vortex shedding, along the span of the cylinder of the 22.5° and 0° cruciforms at $U^*$ = 22.7. 130
Figure 4.40 Dominant vortical structures at $U^*$ = 22.7 observed in the 22.5° and 0° cases. 132
Figure 4.41 The Q-criterion for the 22.5° cruciform at $U^*$ = 4.5: the isometric (4.41a) and plan view (4.41b). 133
Figure 4.42 The Q-criterion for the 22.5° cruciform at $U^*$ = 22.7: the isometric (4.42a) and plan view (4.42b). 134
Figure 4.43 The Q-criterion for the 0° cruciform at $U^*$ = 4.5: the isometric (4.43a) and plan view (4.43b). 134
Figure 4.44 The Q-criterion for the 45° cruciform at $U^*$ = 22.7: the isometric (4.44a) and plan view (4.44b). 135
Figure 4.45 Phase lag $\theta_{y-C_L}$ (°) between $C_L$ and $y^*$ when 22.5° and 0°. 137
Figure 4.46 Isocontours describing the map of the normalised RMS amplitude of cylinder displacment, $y^*_{RMS}$ in the cruciform angle - reduced velocity ($\alpha$–$U^*$) parameter space. 139

Figure 4.47 Isocontours describing the map of the estimated mechanical power in the cruciform angle - reduced velocity ($\alpha$–$U^*$) parameter space. 140
Figure 4.48 Isocontours describing the map of the estimated mechanical efficiency in the cruciform angle - reduced velocity ($\alpha$–$U^*$) parameter space. 141

## LIST OF ABBREVIATIONS

| | | |
|---|---|---|
| 3D | - | Three-dimensional |
| ACMI | - | Arbitrarily Coupled Mesh Interface |
| CFD | - | Computational Fluid Mechanics |
| CFL | - | Courant-Friedrichs-Lewy |
| DKSGS | - | Dynamic k-equation Subgrid-scale |
| DNS | - | Direct Numerical Simulation |
| EMD | - | Empirical Mode Decomposition |
| EEMD | - | Ensemble Empirical Mode Decomposition |
| FIV | - | Fluid-induced Vibration |
| FSI | - | Fluid-structure Interaction |
| GAMG | - | Geometric-Algebraic Multi Grid |
| GCI | - | Grid Convergence Index |
| HT | - | Hilbert Transform |
| HHT | - | Hilber-Huang Transform |
| ICT | - | Information and Communications Technology |
| IF | - | Intrinsic Function |
| KVIV | - | Karman Vortex-induced Vibration |
| MD | - | Molecular Dynamics |
| PISO | - | Pressure-Implicit with Splitting Operators |
| PIMPLE | - | PISO-stabilised SIMPLE |
| PIV | - | Particle Image Velocimetry |
| POD | - | Proper Orthogonal Decomposition |
| PTC | - | Passive Turbulence Control |
| PV | - | Cauchy Principal Value |
| SIMPLE | - | Semi-implicit Method for Pressure Linked Equations |
| SVIV | - | Streamwise Vortex-induced Vibration |
| TrSL | - | Transition in Shear Layer |

| | | |
|---|---|---|
| URANS | - | Unsteady Reynolds Averaged Navier-Stokes |
| VIV | - | Vortex-induced Vibration |

## LIST OF SYMBOLS

| | | |
|---|---|---|
| $a(t)$ | - | Instantaneous amplitude |
| Cl | - | Lift coefficient |
| $C_d$ | - | Drag coefficient |
| $C_{y^*,y^*}$ | - | IMF component of $y^*$ with highest correlation to $y^*$ |
| $C_{Cl,y^*}$ | - | IMF component of $C_L$ with highest correlation to $y^*$ |
| $C_{C_L,RMS}$ | - | Root-mean-square of characteristic IMF of Cl |
| D | - | Characteristic diameter |
| $F_L$ | - | Lift force |
| $F_s$ | - | Safety factor for GCI estimation |
| $f_{cyl.}$ | - | Dominant cylinder vibration frequency |
| $f_{RE}$ | - | Richardson extrapolation of quantity in GCI study |
| $f_n$ | - | Natural system frequency |
| $f_{v,Karman}$ | - | Karman vortex shedding frequency |
| $f^*$ | - | Normalised system frequency |
| $g$ | - | Gap between upstream cylinder and downstream plate |
| $G$ | - | Normalised gap |
| $h$ | - | Average mesh cell size |
| $l_{cylinder}$ | - | Length of upstream cylinder |
| $m_{eff.}$ | - | Effective system mass |
| $O$ | - | Order of magnitude |
| $P$ | - | Pressure |
| $p$ | - | Order of accuracy grid independence study |
| $P_{Fluid,RMS}$ | - | Root-mean-square of fluid power |
| $P_{Mech.,RMS}$ | - | Root-mean-square of mechanical power |
| Re | - | Reynolds number |
| $r^p$ | - | Mesh refinement ratio |
| $S_{grid,\,i}$ | - | Total number of cells in the $i^{th}$ grid |

| | | |
|---|---|---|
| $S_{ij}$ | - | Strain rate |
| St | - | Strouhal number |
| $\mathrm{St}_{\mathrm{Karman}}$ | - | Strouhal number of Karman vortex shedding |
| $T_{\mathrm{osc.}}$ | - | Period of oscillation |
| $t$ | - | Time |
| $U$ | - | Velocity |
| $U_\infty$ | - | Free stream velocity |
| $u'$ | - | Fluctuating component of velocity |
| $U^*$ | - | Reduced velocity |
| $\mathrm{V_{in}}$ | - | Input voltage |
| $W_{\mathrm{Cl}}$ | - | Mean work done over one vibration cycle |
| $y$ | - | Vertical cylinder displacement |
| $y^*$ | - | Normalised vertical cylinder displacement |
| $y^*_{\mathrm{RMS}}$ | - | Root-mean-square of vertical cylinder displacement |
| $\beta$ | - | Porosity |
| $\delta$ | - | Logarithmic damping |
| $\lambda$ | - | Mesh deformation velocity and displacement diffusion |
| $\nu$ | - | Kinematic viscosity |
| $\nu_T$ | - | Kinetic eddy viscosity |
| $\omega(t)$ | - | Instantaneous frequency |
| $\phi$ | - | Representative phase lag between $y$ and Cl |
| $\theta y - \mathrm{Cl}$ | - | Phase lag between $y$ and Cl |
| $\partial$ | - | Partial differential operator |
| $\rho$ | - | Fluid density |
| $\tau$ | - | Reynolds stress tensor |
| $\theta(t)$ | - | Instantaneous phase |
| $\zeta_{\mathrm{tot.}}$ | - | Total damping coefficient |

## LIST OF APPENDICES


| APPENDIX | TITLE | PAGE |
|---|---|---|
| Appendix A | Temporal Evolution of Lift in a Pure Cruciform System for Energy | 161 |
| Appendix B | OpenFOAM Implementation for The Study of Streamwise Vortex-Induced Vibration-Based Energy Harvester for Sensor Networks | 162 |

# CHAPTER 1

# INTRODUCTION

This chapter gives the reader a brief overview of the contents of the thesis. The chapter begins with the Section 1.1 Background of Study. Here, an abridged introduction to the topic of flow-induced vibration (FIV) is provided, specifically, on vortex-induced vibration (VIV) for energy harvesting. Two types of VIV are discussed: Karman VIV and streamwise VIV. This is followed by the prerequisites of their formation and the pros and cons of each in terms of energy harvesting.

Next, the chapter proceeds with Section 1.2, Problem Statement. This lists the main gaps to be closed in this thesis. Then, Section 1.3, Research Questions translates the gaps identified in the preceding section into concrete questions that this work will address in subsequent chapters. Following this, the Thesis Objectives are listed in Section 1.4 and Significance of Study in Section 1.6. Finally, the chapter explains the Scope of Work in 1.5 and ends with the outline of the thesis in Section 1.7, Thesis Organisation.

## 1.1 Background of Study

The term "flow-induced vibration" refers to a wide range of phenomena. One of the phenomenon is called flutter, which is the flapping of a thin, flexible structure that results from the competition between periodic bending forces due to the shedding of vortices, and the stabilising forces from the structure itself (Xia *et al.*, 2015). Another example is galloping, which is the outcome of aeroelastic instability of an elastically supported cylinder (Kluger *et al.*, 2013). On the other hand, vibration of a structure due to resonance with the frequency of turbulent eddies around it is called turbulence-induced vibration (Nakamura *et al.*, 2013). Finally, there are also structural vibrations that are the result of excitations coming from the wake of another structure, named wake-induced vibration (Derakhshandeh *et al.*, 2014). The vast majority of these

phenomena were studied as part of a program to suppress the vibrations, to prevent structural failure (Khalak and Williamson, 1999).

On the other hand, vortex-induced vibration (VIV) is a type of vibration that grows from instabilities in fluid flows moving past a solid object, i.e. bluff body. When the flow exceeds a critical velocity, the flow develops vortices that are shed alternately downstream the bluff body. This triggers the onset of unsteady lift and drag forces that initiate and sustain its vibration (Bukka *et al.*, 2020). The common denominator for all these examples is the potential damage to the engineering construct experiencing it. Thus, methods are devised and implemented to mitigate the effects of the vibrations by dissipating the vibrational energy or delaying/aborting its onset in the first place.

However, the past decade has seen efforts to instead make the vibration stronger. For example, purposefully maximising the vibration of flexible piezoelectric flags to harvest wind energy from low-speed winds (Mehdipour *et al.*, 2022). Another example is the effort to maximise the vibration of in-tandem VIV nanogenerators for energy harvesting by (Zhang *et al.*, 2022b). Simple circular cylinder oscillators has also been studied to increase its vibration amplitude and efficiency in energy conversion (Zhang *et al.*, 2022a). The simplicity of design and scalability attracts many to contribute to this multidisciplinary field of study, along with the prospect of successful development and subsequent commercialization of a new generation of energy harvesters. Also, technical publications since the 2000s saw a surge in contributions toward the subject from the perspective of energy harvesting. A simple search in SCOPUS shown in Fig. 1.1 reveals this trend for keywords [“vortex induced vibration” energy] for the last 4 decades.

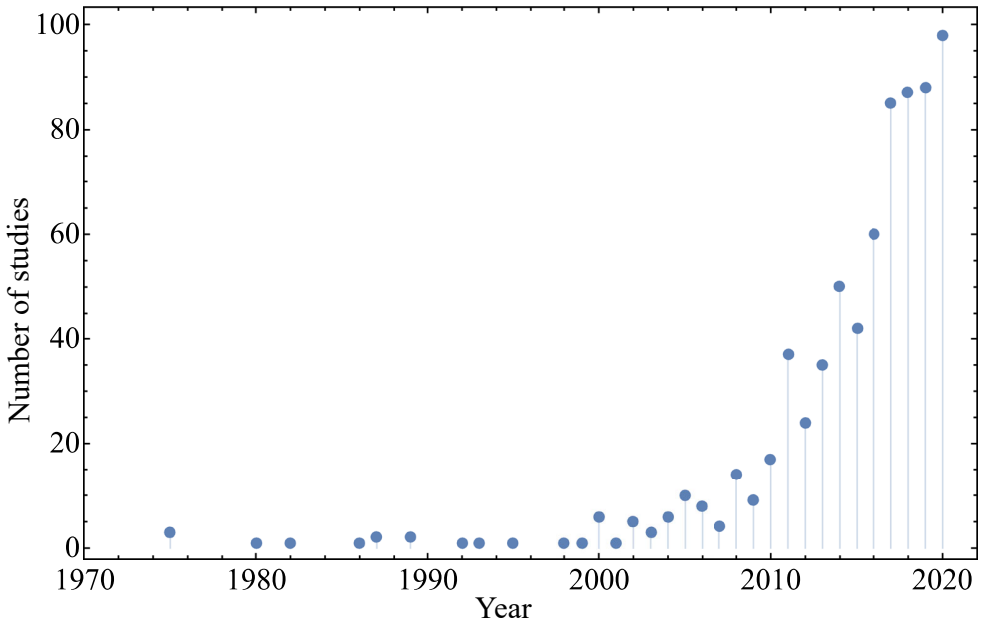


Figure 1.1 Number of publications with keywords ["vortex induced vibration" energy]. Retrieved from SCOPUS.

At the cutting edge of this field of research is a group at The University of Michigan, that has already built prototypes of the energy harvester, named VIVACE (**v**ortex-**i**nduced **v**ibration for **a**quatic **c**lean **e**nergy). They compared the cost of power production in USD/kWh between VIVACE and a wide selection of common (pulverised coal, integrated gasification combined cycle, natural gas combined cycle, etc.) and new power generation technologies (anaerobic digester, landfill gas, solar, etc.). In doing so, they found that VIVACE is on par in terms of power production cost with the other conventional technologies, and published their findings in Bernitsas *et al.* (2008). This result demonstrated VIVACE's economic appeal.

The VIV phenomenon utilised by the team at the University of Michigan is of the Karman VIV type (KVIV), capable of producing power in the order of MW when installed as a large-scale energy farm (Raghavan, 2007). Karman VIV - or KVIV for short - is a form of VIV that is induced and sustained by the periodic shedding of Karman vortices from opposite surfaces of a cylinder. The periodic shedding of these vortices creates a pressure fluctuation from the opposing surfaces (Mei *et al.*, 2021). This produces a net fluctuating force acting on the cylinder, which is the lift that

drives its vibration. Karman vortices fall into the category of spanwise vortices, and structurally, a single cylinder is all one needs to trigger its formation (Liu *et al.*, 2022).

However, as pointed out by Koide *et al.* (2013) the reduced velocity ($U^*$) range within which KVIV can be relied upon for power generation is about one order of magnitude smaller than what can be expected from another form of VIV namely the streamwise VIV (SVIV). Reduced velocity $U^*$ is a nondimensional characteristic velocity that allows comparison of results between similar systems vibrating in a flow. Reduced velocity is defined as follows.

$$U^* = \frac{U_\infty f_n}{D}, \tag{1.1}$$

where $U_\infty$, $f_n$ and $D$ refers to the freestream velocity, natural frequency of the system and diameter of the cylinder respectively. Using $U^*$ to express flow velocity allows the reader to gauge how fast the flow is, with respect to the speed of vibration at $f_n$.

Streamwise VIV - or SVIV for short - has its vorticity vector parallel to the direction of the flow. This is different from KVIV whose vorticity vector is perpendicular to the direction of the flow, and is instead parallel to the axis of the cylinder. Structurally, unlike a single cylinder like KVIV, SVIV needs two cylinders in cruciform to trigger its formation. This cruciform is made by placing one cylinder upstream and another downstream. The axes of the two cylinders are at right angles to each other. The midpoint of the cylinders overlap one another, forming a plus sign, i.e. "+". This type of cruciform, where the two cylinders are at 90° to each other is called the pure cruciform.

Streamwise vortices that drive the vibration of the cylinder appear in pairs, one on the left, and another on the right of the "+". The streamwise vortex on the left of the "+" rotates in the opposite direction to the streamwise vortex on the right. This means that the streamwise vortex pair is a counter-rotating pair of vortex. This counter-rotation produces the alternating lift on the upstream cylinder. Since SVIV power generation is

possible for a large range of $U^*$, it is better suited for deployment in flows with large velocity changes.

Unlike KVIV-based energy harvesters, the oscillating upstream cylinder of SVIV-based energy harvesters have both Karman and streamwise vortices shed from it (Koide *et al.*, 2017). This presents a challenge to the measurement of the phase lag between the lift and vibration signals. The closer the phase lag is to 90°, the higher the power output (Koide *et al.*, 2013; Raghavan, 2007). Hence it is favourable to be able to measure the phase lag as it can help explain an observed improvement or deterioration of the power output. Since both Karman and streamwise vortices are shed from SVIV-based energy harvesters, distinguishing which part of the lift signal is due to either, is difficult. A time-resolved signal processing method is needed and in this study, the Hilbert-Huang Transform (HHT) analysis is employed.

The HHT analysis involves two steps: the first is decomposing a time-series signal into components of decreasing mean frequency, and second, to apply the Hilbert transform on the components to obtain the instantaneous phase (de Souza *et al.*, 2022). The application of HHT analysis enables this work to distinguish the dominant components of the lift signal, identify which of these is actually driving the vibration of the cylinder, and compute its phase lag against the vibration signal.

One shortcoming of a SVIV-based harvester is its maximum power output which is demonstrated at the current stage of development to cap at a mW scale for a single-cylinder setup. An isolated cylinder setup for KVIV produces a maximum power in the order of 10 W (Bernitsas *et al.*, 2009). The apparent power $P_a$ (W) for both KVIV and SVIV is shown in Fig. 1.2. Following this present limitation of the unoptimized SVIV energy harvesters, their application is currently limited to mW electronics e.g., sensors and signal transmitters.

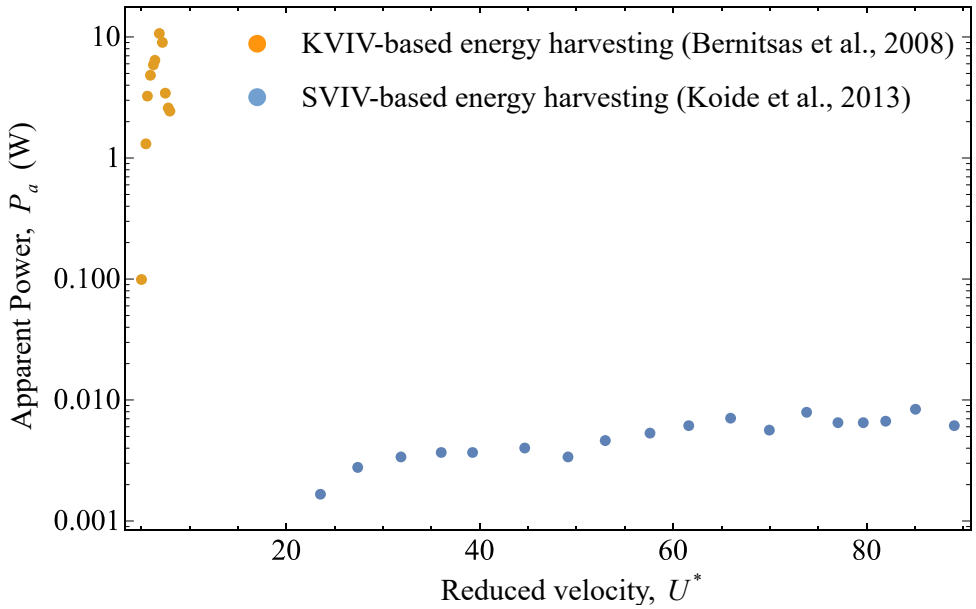


Figure 1.2 Apparent power $P_a$ (W) versus reduced velocity $U^*$ for cases of KVIV and SVIV. Adapted from Koide *et al.* (2013).

Nevertheless, these sensors and signal transmitters can make up environment-monitoring sensor networks to monitor the water level in rivers and irrigation canals that benefit flood forecasting efforts. The sensor network can also be used to monitor the level of pollution of the river or canal. This is possible by installing concentration sensors for specific contaminants. Finally, low-power batteries can also benefit from this energy harvesting technology, especially in the context of off-grid charging.

To expand the usability of the cruciform oscillator in energy harvesting, efforts should be made to improve its power output. Hence, this thesis seeks to identify the causes that limits the power output to its current value. This includes the identification of vortical structures in the flow, their location, and strength. The thesis also looks into the modulation of the lift signal by the shedding of vortical structures. Then, this thesis seeks to explore a new parameter in the study of the cruciform oscillator, which is the cruciform angle. This study documents the effects of the various cruciform angles on the vortical structures present in the flow in terms of their location and strength. In addition, this work also studies their effects on the lift and vibration signal, and ultimately, estimated power output and efficiency.

## 1.2 Problem Statement

The preceding section has established the viability of harnessing energy from a flow by exploiting the VIV phenomenon. Multiple modes of VIV have been observed, and SVIV stands out as better oriented for deployment in fluid flows that vary greatly in terms of free-stream velocity. Even with very rudimentary optimisations, SVIV from a cruciform harvester has the ability to generate power in the order of mW consistently over a large range of free-stream velocities (Koide *et al.*, 2013).

To achieve this, the problems outlined below must be addressed to close relevant gaps in the current body of knowledge.

1. A lack of understanding on the transition mechanism from Karman to streamwise vortex-induced vibration.
2. A paucity in the knowledge on what contributes to the magnitude of the alternating lift force acting on the cylinder, and its vibrational frequency components.
3. A deficiency of new methods to control the flow perturbation which gives rise to a strong, stable and periodic forcing of the cylinder vibration, sustainable over the desired operating range of $U^*$.

Problem statement one stems from the realisation that although past studies have shown that SVIV in a cruciform harvester begins around $U^* = 18$ (Koide *et al.*, 2013), none has ever looked into how the transition actually occurs from KVIV. This is especially the case in terms of the distribution of vortical structures around the cruciform, the lift signal: its frequency, amplitude and phase lag relative to the cylinder vibration signal. Removing this lack of understanding can help to trigger the desired mode of vibration at a lower $U^*$.

Problem statement two stems from the observation by Zhao and Lu (2018) on sectional lift, which drew attention to the effect a vortical structure has on the lift acting on the cylinder. Particularly in the case where several types of vortices are being shed simultaneously - like the cruciform harvester - the paucity in the knowledge on how

the different vortical structures affect the lift signal is a hindrance to improving the maximum lift that can be possible obtained from the cruciform harvester.

Finally, problem statement three comes from the realisation that recent studies in the field of cruciform energy harvester seems to be hard-pressed in finding new parameters to explore, focusing time and again on the gap between the cylinder and the downstream plate, the plate width and other dimensions of the system (Sakamoto *et al.*, 2021).

To date, the upstream and downstream cylinder (or plate) in cruciform harvesters have always been assumed to be at 90° to each other. It is possible that keeping the cruciform at a right angle prevents the discovery of other configurations that are capable of outputting higher power at better efficiencies. With enough cruciforms studied between angles 0° and 90°, one can synthesise a map of power and efficiency of cruciform harvesters at various cruciform angles $\alpha$ (°) that can advise on the selection of the cruciform harvester for a given design constraint.

### 1.3 Research Questions

The answer to several questions is sought in this proposed study. These questions are meant to drive the study towards its objectives.

1. How does the lift signal evolve as the flow transitions from being driven primarily by Karman vortex to streamwise vortex?
2. How does the ratio of energy transferred from the flow to the lift components evolve with respect to $U^*$?
3. Compared to a pure cruciform, what are the differences the Karman or streamwise vortical structures experience under the condition of a modified cruciform?
4. How do the differences mentioned in 3 affect the lift magnitude, and by extension the frequency-amplitude response?

5. Where in the power envelope can maximum (minimum) power be obtained with the largest (narrowest) operability range, and how does this translate into a new mode of flow control to suit the operating conditions of the cruciform energy harvester?

## 1.4 Thesis Objectives

Following the problems outlined in the previous section, the objectives that define the scope of work in this proposal are listed below.

1. To identify the causes of the difference in amplitude and frequency response of the lift and vibration signals when the dominant vortical structure changes from Karman to streamwise vortex, in a pure cruciform.
2. To distinguish the dominant components of the lift signal and how the components interact to modify the amplitude and frequency response of cylinder vibration, in a pure cruciform.
3. To synthesise a map for each of the amplitude, power, and efficiency, summarised in the cruciform angle $\alpha$ (°) - reduced velocity $U^*$ parameter space.

As mentioned previously in Section 1.2, there is a lack of understanding on how the transition from KVIV to SVIV takes place in a cruciform energy harvester, which is the first problem statement. The first objective is thus to establish the relationship between the amplitude and frequency response of the lift and vibration signals and the vortical structures that are present at that time. The amplitude response is computed by taking the root-mean-square of the signals, both lift and vibration, and plotting them against $U^*$. The frequency response is computed by finding the dominant frequency in the FFT spectrum of the signals, both lift and vibration. Vortical structures are identified by computing the vorticity field.

Then, the second objective of distinguishing the dominant components of the lift signal is to answer problem statement two. As the reason behind the modulation of the lift signal remains unknown, this objective seeks to analyse the lift signal. The

method of analysis to be employed here is HHT, through which the signal can be decomposed and the dominant components identified. Once the components of lift have been identified, the study can explain how they interact to produce the amplitude and frequency response of the cylinder vibration being observed.

Lastly, the third objective of synthesising a map of the vibration amplitude, power and efficiency in the $\alpha$ (°) - reduced velocity $U^*$ parameter space is stated to answer problem statement three. As mentioned in problem statement three, the fact that studies have always assumed the cruciform oscillator to have a cruciform angle of 90° has prevented the investigation of a generalised cruciform oscillator. By computing the amplitude response, power and efficiency of a few cruciforms between $0 \leq \alpha\ (°) < 90$, this study will be able to evaluate the feasibility of varying the angle of the cruciform as a method to control flow perturbations due to the arrangement of vortical structures around the cruciform. This also provides a guideline for the optimal cruciform angle for a given design constraint such as vibration clearance, structural integrity and operating range of $U^*$, in addition to power output and efficiency.

## 1.5 Scope of Works

This work is a mainly a computational fluid dynamics (CFD) study of a particular version of VIV-based energy harvester that comprises of an elastically supported, horizontally constrained smooth circular cylinder of diameter 1 cm and a passive flow control mechanism that is a strip of rectangular plate at a right angle downstream the cylinder, forming a cruciform. The range of Reynolds number investigated in this thesis is between $1.1\times10^3 \leq \mathrm{Re} \leq 14.6\times10^3$ and the mass-damping parameter, expressed by the nondimensional Scruton number Sc, is 9.94. This work limits itself to examining a cruciform where the width of the strip plate is equal to the diameter of the cylinder $D$, and the primary data collected from the simulation runs are the time evolution of the cylinder displacement and the corresponding lift coefficient $\mathrm{C_L}$.

The baseline numerical results, i.e. results from a pure cruciform (a cruciform where the cylinder and strip plate are 90° to each other) are validated against experimental results of a similar system in a custom-made recirculating open flow

channel. This experiment to validate the baseline numerical results also used a 1 cm diameter circular cylinder. A strip plate of width 1 cm was placed downstream the circular cylinder at a 90° angle. Data collected from the experiment is limited to the vibration signal (i.e., cylinder displacement) only, and only between $1.1 \times 10^3 \leq \text{Re} \leq 11.2 \times 10^3$. The vibration signal is then post-processed into their respective amplitude and frequency responses.

The simulation in this study collects data on the three-dimensional pressure and velocity fields, and also cylinder displacement data. The pressure field is then post-processed to obtain lift signal acting on the cylinder, while the velocity field is post-processed to obtain the vorticity field. This is in relation to objective one that seeks to establish the amplitude and frequency responses of the lift and cylinder vibration signals. This is different from the parameters studied in Koide *et al.* (2017), as in their experiment, they only seeked to visualise the different vortical structures that appear between $1.2 \times 10^3 \leq \text{Re} \leq 5.7 \times 10^3$ for cruciforms with different cross-sectional shapes.

On the other hand, the study by Zhao and Lu (2018) only looked into the visualisation of the vortical structures around the cruciform and the distribution of lift along the vibrating cylinder. The range of Reynolds number they studied was between $1 \times 10^2 \leq \text{Re} \leq 5 \times 10^2$. This distribution of lift along the length of the vibrating cylinder reveals the location of dominant vortical structures and helps to visualise their strength with respect to time. Instead, this thesis used the FFT of the transverse (direction parallel to the vibration of the cylinder) velocity component downstream the cylinder to visualise dominant vortical structures and their strength.

This thesis looks to discover the relationship between the vortical structures present in the flow and how they modulate the resulting lift acting on the vibrating cylinder of the pure cruciform. Special focus is given to the high flow velocity region where SVIV takes place. This is done by conducting a time-series analysis of both cylinder displacement and lift coefficient signals using the Hilbert-Huang transform (HHT). The motivation behind this is to understand why the amplitude of cylinder displacement is limited to the order of magnitude observed not only by the author, but

also in numerous studies within the last ten years. This part of the study concludes with the discovery of a particular route through which a significant amount of energy from the freestream is lost during the energy harvesting process, and the amount by which the power output can be improved if this loss is eliminated. This scope is related to objective two.

The second part of this thesis is the author's attempt to eliminate the loss mentioned previously. This is done by generalising the cruciform system, through the variation of the relative angle between the cylinder and the strip plate. The study then proceeds to investigate the generalised cruciform system by examining the vortical structures present in the flow, how they affect the resulting lift acting on the cylinder, the amplitude of cylinder displacement itself, and ultimately the power output. The dynamics between the lift and cylinder displacement are explained through the computation of instantaneous phase lag between the two, which in turn is made possible by HHT.

The thesis concludes with the unveiling of a mechanical power and efficiency map, within a parameter space consisting of the cruciform angle and $U^*$. Useful recommendations can be deduced from the map, which highlights regions of high and low power output, and also regions of high and low efficiency, in order to obtain the desired power output and efficiency for any given power consumption requirement. This scope is related to objective three.

## 1.6 Significance of Study

The aim of objective one is to get a better understanding on SVIV in a pure cruciform. A better understanding of SVIV in a pure cruciform in important because this is the baseline case, to which the performance of other cruciforms at different cruciform angles will be compared. Achieving this objective can demonstrate how the inception of streamwise vortical structures perturb the amplitude and frequency of lift, which directly modifies the amplitude and frequency of the cylinder vibration.

Next, achieving objective two is desirable because it allows the establishment of a direct link between the different branches of KVIV or SVIV and how the vortices modulate the lift signal of a pure cruciform. Apart from that, distinguishing the dominant components of lift allows us to quantify how much energy from the flow is consumed by each of the Karman or streamwise vortices, and in return, how much do they contribute towards driving the vibration of the cylinder. Investigating this for the pure cruciform lay the grounds to understand how power generation is affected by the configuration of vortices in the flow for more complex situations, i.e., when the cruciform angle is no longer 90°.

Finally, objective three is significant because in achieving it, one is able to evaluate and recommend the optimal cruciform angle for the designated specifications for vibration clearance, power output and efficiency. This holds the key as to how the cruciform angle should be varied to cater to a particular flow environment and structural integrity - much like the performance curves associated with engines and pumps.

## 1.7 Thesis Organisation

This thesis is organised into eight chapters. The author introduces the study and gives a general overview of the research in Chapter One. In Chapter One, gaps in the research are identified and thesis objectives are formulated based on those gaps. Chapter One also outlines the questions the author seeks to address, details the scope of this study and provide concrete examples as to the significance and merit of this work. Chapter Two reviews relevant literature that gives an overview of the progress made up to the present day, on the subject of VIV energy harvesting, by exploiting an isolated circular cylinder as the oscillator. The chapter then introduces the cruciform oscillator and the studies on the vibration characteristics of a number of variations of the cruciform oscillator.

Chapter Three discusses the methodology taken by the author to attain the objectives listed in Chapter One. In Chapter Three, the author details the numerical model implemented in the CFD undertaking and this includes the domain size, critical dimensions of the cruciform, boundary conditions and solution method to the unsteady,

three-dimensional (3D) Reynolds-averaged Navier-Stokes equation governing the flow. Apart from that, the author also discusses the turbulence modelling adhered to in the numerical studies. The author also introduces the Hilbert-Huang transform (HHT) and explains the ensemble empirical mode decomposition (EEMD) algorithm that drives the decomposition of a time series signal into a finite number of orthogonal components. Finally, the author explains the Hilbert transform and how the transform is able to compute instantaneous phase or frequencies of a decomposed component of the signal.

Chapter Four first takes into account the validation of the numerical setup in two ways: by way of a grid independency study, and by way of experimental comparison. The grid independency study utilises the Richardson extrapolation and grid convergence index (GCI) as the primary tool to ensure spatial convergence of the numerical results. In the experimental validation, this work showcases a simple contactless method of measuring the cylinder displacement using a camera and an open-source image tracking software. After the processing of the experimental data to compute the uncertainty and present them as error bars, the author concluded that the numerical results of the pure cruciform (90° cruciform) is in fair agreement with the experimentally obtained values, providing an added layer of confidence in the numerical results.

This is then followed by the vibration characteristics of a pure cruciform. In this section, the author studies in detail the lift-displacement dynamics that results from the kind of vortical structures that appear in this setup. This section concludes with the discovery of a path to energy loss that has never been considered before in the literature and estimated the amount of improvement possible for the power output if said loss is eliminated.

Then, the chapter continues to discuss the vortical structures and lift-displacement dynamics of a steep-angled cruciform ($45 \leq \alpha(^\circ) \leq 67.5$), followed by the vortical structures and lift-displacement dynamics of a shallow-angled cruciform ($0 \leq \alpha(^\circ) \leq 22.5$). Here, the study found out that for shallow-angled cruciforms, the onset of meaningful power generation is brought down significantly to from $U^* = 18.2$ in the pure cruciform, to $U^* = 9.1$ when the cruciform angle is 0°. At $\alpha = 0^\circ$, the maximum power also improves by approximately a factor of two.

Finally, the author computes the mechanical power and efficiency of each of the cruciform variants for all flow velocities studied. From it, this work is able to produce a mechanical power and efficiency map, in essentially a cruciform angle-flow velocity parameter space.

Chapter Five details the conclusions that follow the discussions made in Chapter Four. Here, the four main findings of this work are summarised and the chapter ends with some remarks on potential future works for this study.

# REFERENCES


Adzlan, A., Mat Ali, M. S. and Zaki, S. A. (2021). Temporal evolution of lift in a pure cruciform system for energy harvesting. *Ocean Engineering*. 223, 108648. ISSN 00298018. doi:10.1016/j.oceaneng.2021.108648.

Agbaglah, G. and Mavriplis, C. (2019). Three-dimensional wakes behind cylinders of square and circular cross-section: Early and long-time dynamics. *Journal of Fluid Mechanics*. 870, 419–432. ISSN 1469-7645. doi:10.1017/jfm.2019.265.

Alves Portela, F., Papadakis, G. and Vassilicos, J. C. (2020). *The role of Coherent Structures and Inhomogeneity in Near-Field Inter-Scale Turbulent Energy Transfers*.

Arsh, B. A. (2020). Advances in the smart materials applications in the aerospace industries. *Aircraft Engineering and Aerospace Technology*. 92(7), 1027–1035. ISSN 1748-8842. doi:10.1108/AEAT-02-2020-0040.

Asano, Y., Watanabe, H. and Noguchi, H. (2020). Effects of cavitation on Kármán vortex behind circular-cylinder arrays: A molecular dynamics study. *Journal of Chemical Physics*. 152(3), 034501. ISSN 0021-9606. doi:10.1063/1.5138212.

Bae, H. M., Baranyi, L., Koide, M., Takahashi, T. and Shirakashi, M. (2001). Suppression of Karman Vortex Excitation of a Circular Cylinder By a Second Cylinder set Downstream in Cruciform Arrangement. *Journal of Computational and Applied Mechanics*. 2(2), 175–188. ISSN 0717-6163. doi:10.1007/s13398-014-0173-7.2.

Barati, E., Biabani, M. and Zarkak, M. R. (2022). Numerical investigation on vortex-induced vibration energy harvesting of a heated circular cylinder with various cross-sections. *International Communications in Heat and Mass Transfer*. 132, 105888. ISSN 0735-1933. doi:10.1016/J.ICHEATMASSTRANSFER.2022.105888.

Bernitsas, M. and Raghavan, K. (2008a). Reduction/suppression of VIV of circular cylinders through roughness distribution at $8\times10^3 < \mathrm{Re} < 1.5\times10^5$. In *Proceedings of the International Conference on Offshore Mechanics and Arctic Engineering - OMAE*, vol. 5. July.

Bernitsas, M. and Raghavan, K. (2008b). Reduction/suppression of VIV of circular cylinders through roughness distribution at $8\times10^3 < \mathrm{Re} < 1.5\times10^5$. In *Proceedings of the International Conference on Offshore Mechanics and Arctic Engineering - OMAE*, vol. 5. July. ISBN 9780791848227.

Bernitsas, M. M., Ben-Simon, Y., Raghavan, K. and Garcia, E. M. H. (2009). The VIVACE Converter: Model Tests at High Damping and Reynolds Number Around $10^5$. *Journal of Offshore Mechanics and Arctic Engineering*. 131(1). ISSN 0892-7219. doi:10.1115/1.2979796.

Bernitsas, M. M., Raghavan, K., Ben-Simon, Y. and Garcia, E. M. H. (2008). VIVACE (Vortex Induced Vibration Aquatic Clean Energy): A New Concept in Generation of Clean and Renewable Energy From Fluid Flow. *Journal of Offshore Mechanics and Arctic Engineering*. 130(4), 041101. ISSN 0892-7219. doi:10.1115/1.2957913.

Bhukta, M. K., Bose, G. K. and Debnath, K. (2018). Study of turbulent plane circular jet for modulation of recirculation zone behind a cubical obstruction. *Advanced Applications in Manufacturing Engineering*, 231–249. doi:10.1016/B978-0-08-102414-0.00008-2.

Blevins, R. D. (1990). Flow-induced vibration.

Bukka, S. R., Magee, A. R. and Jaiman, R. K. (2020). Stability analysis of passive suppression for vortex-induced vibration. *Journal of Fluid Mechanics*. ISSN 1469-7645. doi:10.1017/jfm.2019.1026.

Chen, H., Meng, C., Shan, Z., Fu, Z. and Bhargava, B. K. (2019). A novel low-rate denial of service attack detection approach in zigbee wireless sensor network by combining hilbert-huang transformation and trust evaluation. *IEEE Access*. ISSN 21693536. doi:10.1109/ACCESS.2019.2903816.

de Souza, U. B., Escola, J. P. L. and Brito, L. d. C. (2022). A survey on Hilbert-Huang transform: Evolution, challenges and solutions. *Digital Signal Processing*. 120, 103292. ISSN 1051-2004. doi:10.1016/J.DSP.2021.103292.

Deng, J., Ren, A.-L. and Shao, X.-M. (2007). The flow between a stationary cylinder and a downstream elastic cylinder in cruciform arrangement. *Journal of Fluids and Structures*. 23(5), 715–731. ISSN 0889-9746. doi:10.1016/J.JFLUIDSTRUCTS.2006.11.005.

Derakhshandeh, J. F., Arjomandi, M., Dally, B. and Cazzolato, B. (2014). The effect of arrangement of two circular cylinders on the maximum efficiency of Vortex-Induced Vibration power using a Scale-Adaptive Simulation model. *Journal of Fluids and Structures*. 49, 654–666. doi:10.1016/j.jfluidstructs.2014.06.005.

Desai, A., Mittal, S. and Mittal, S. (2020). Experimental investigation of vortex shedding past a circular cylinder in the high subcritical regime. *Physics of Fluids*. 32(1), 014105. ISSN 1089-7666. doi:10.1063/1.5124168.

Ding, L., Zhang, L., Kim, E. S. and Bernitsas, M. M. (2015a). URANS vs. experiments of flow induced motions of multiple circular cylinders with passive turbulence control. *Journal of Fluids and Structures*. 54, 612–628. ISSN 1095-8622. doi: 10.1016/j.jfluidstructs.2015.01.003.

Ding, L., Zhang, L., Wu, C., Mao, X. and Jiang, D. (2015b). Flow induced motion and energy harvesting of bluff bodies with different cross sections. *Energy Conversion and Management*. ISSN 0196-8904. doi:10.1016/j.enconman.2014.12.039.

Ding, W., Sun, H., Xu, W. and Bernitsas, M. M. (2017). Two tandem cylinders with turbulence stimulation in FIV power conversion: CFD with experimental verification of interaction. In *Proceedings of the International Conference on Offshore Mechanics and Arctic Engineering - OMAE*, vol. 10. September. doi: 10.1115/OMAE2017-62271.

Ding, W., Sun, H., Xu, W. and Bernitsas, M. M. (2019). Numerical investigation on interactive FIO of two-tandem cylinders for hydrokinetic energy harnessing. *Ocean Engineering*. 187, 106215. doi:10.1016/J.OCEANENG.2019.106215.

Duranay, A. and Kinaci, O. K. (2020). Enhancing two-dimensional computational approach for vortex-induced vibrations by scaling lift force. *Ocean Engineering*. 217, 107620. ISSN 0029-8018. doi:10.1016/j.oceaneng.2020.107620.

Durhasan, T., Pinar, E., Ozkan, G., Akilli, H. and Sahin, B. (2019). The effect of shroud on vortex shedding mechanism of cylinder. *Applied Ocean Research*. 84, 51–61. ISSN 0141-1187. doi:10.1016/j.apor.2019.01.007.

Feng, C. C. (1963). The measurement of vortex idunced effects in flow past stationary and oscillating circular and D-section cylinders. (October), 100.

Garcia, E. M. and Bernitsas, M. M. (2018). Effect of damping on variable added mass and lift of circular cylinders in vortex-induced vibrations. *Journal of Fluids and Structures*. 80, 451–472. ISSN 0889-9746. doi:10.1016/J.JFLUIDSTRUCTS.2018.02.005.

Geyer, T. F. (2020). Vortex shedding noise from finite, wall-mounted, circular cylinders modified with porous material. *AIAA Journal*. 58(5), 2014–2028. ISSN 0001-1452. doi:10.2514/1.J058877.

Gibeau, B. and Ghaemi, S. (2019). The mode B structure of streamwise vortices in the wake of a two-dimensional blunt trailing edge. *Journal of Fluid Mechanics*. 884. ISSN 1469-7645. doi:10.1017/jfm.2019.931.

Gibeau, B., Koch, C. R. and Ghaemi, S. (2018). Secondary instabilities in the wake of an elongated two-dimensional body with a blunt trailing edge. *Journal of Fluid Mechanics*. 846, 578–604. ISSN 1469-7645. doi:10.1017/jfm.2018.285.

Gómez-Ortega, O., Landeira, M., Ogueta-Gutiérrez, M., Franchini, S., Sanz-Andres, A., Chimeno, M., Roibás-Millán, E. and Garcia-Perez, A. (2019a). Transverse aeroelastic instability of guard cables with beacons excited by a longitudinal wind. *Journal of Fluids and Structures*. 84, 122–139. ISSN 0889-9746. doi:10.1016/J.JFLUIDSTRUCTS.2018.10.003.

Gómez-Ortega, O., Manzanares-Bercial, R., Ogueta-Gutiérrez, M., Lopez-Nuñez, E., Franchini, S., Roibás-Millán, E. and Sanz-Andres, A. (2019b). Experiments on the transverse aeroelastic instability of a single sphere in a swing configuration under a longitudinal wind. *Journal of Wind Engineering and Industrial Aerodynamics*. ISSN 0167-6105. doi:10.1016/j.jweia.2019.103979.

Hemsuwan, W., Sakamoto, K., Nakada, S. and Takahashi, T. (2018a). A longitudinal vortex wind turbine: Numerical study. *Journal of Wind Engineering and Industrial Aerodynamics*. 180, 213–230. ISSN 0167-6105. doi:10.1016/J.JWEIA.2018.07.022.

Hemsuwan, W., Sakamoto, K., Nakada, S. and Takahashi, T. (2018b). A longitudinal vortex wind turbine: Numerical study. *Journal of Wind Engineering and Industrial Aerodynamics*. 180, 213–230. ISSN 0167-6105. doi:10.1016/J.JWEIA.2018.07.022.

Hemsuwan, W., Sakamoto, K. and Takahashi, T. (2018c). Lift Force Generation of a Moving Circular Cylinder with a Strip-Plate Set Downstream in Cruciform

Arrangement: Flow Field Improving Using Tip Ends. *International Journal of Aeronautical and Space Sciences*. 19(3), 606–617. ISSN 2093-274X. doi: 10.1007/s42405-018-0068-5.

Hemsuwan, W., Sakamoto, K. and Takahashi, T. (2018d). Numerical investigation of lift-force generation on a moving circular cylinder in a uniform flow driven by longitudinal vortex. *Journal of Fluids and Structures*. 83, 448–470. ISSN 0889-9746. doi:10.1016/J.JFLUIDSTRUCTS.2018.09.010.

Hemsuwan, W., Sakamoto, K. and Takahashi, T. (2021). Steady lift-force generation on a circular cylinder utilising a longitudinal vortex: Influence of geometrical parameters. *Journal of Wind Engineering and Industrial Aerodynamics*. 212, 104612. ISSN 01676105. doi:10.1016/j.jweia.2021.104612.

Hu, G. and Kwok, K. C. (2020). Predicting wind pressures around circular cylinders using machine learning techniques. *Journal of Wind Engineering and Industrial Aerodynamics*. 198, 104099. ISSN 0167-6105. doi:10.1016/j.jweia.2020.104099.

Huang, N. E., Shen, Z., Long, S. R., Wu, M. C., Snin, H. H., Zheng, Q., Yen, N. C., Tung, C. C. and Liu, H. H. (1998). The empirical mode decomposition and the Hubert spectrum for nonlinear and non-stationary time series analysis. *Proceedings of the Royal Society A: Mathematical, Physical and Engineering Sciences*. ISSN 1364-5021. doi:10.1098/rspa.1998.0193.

Jeong, J. and Hussain, F. (1995). Hussain, F.: On the identification of a vortex. JFM 285, 69-94. *Journal of Fluid Mechanics*. 285, 69 – 94. doi:10.1017/S0022112095000462.

Kang, Y., Xiao, W., Wang, Q., Zhang, D. and Zhao, J. (2020). Suppression of Vortex-Induced Vibration by Fairings on Marine Risers. *Journal of Ocean University of China*. 19(2), 298–306. ISSN 1672-5182. doi:10.1007/s11802-020-4033-0.

Kato, N., Koide, M., Takahashi, T. and Shirakashi, M. (2006). Influence of Cross-Sectional Configuration on the Longitudinal Vortex Excitation of the Upstream Cylinder in Cruciform Two-Cylinder System. *Journal of Fluid Science and Technology*. 1(2), 126–137. ISSN 1880-5558. doi:10.1299/jfst.1.126. Retrievable at `http://joi.jlc.jst.go.jp/JST.JSTAGE/jfst/1.126?from=CrossRef`.

Kato, N., Koide, M., Takahashi, T. and Shirakashi, M. (2007). Vibration Control for a Circular Cylinder by a Strip-plate Set Downstream in Cruciform Arrangement (1st

Report, Influence of a Downstream Strip-plate on the Shedding of Longitudinal Vortices from Fixed System). *Transactions of the Japan Society of Mechanical Engineers Series B*. 73(728), 957–964. ISSN 0387-5016. doi:10.1299/kikaib.73.957.

Khalak, A. and Williamson, C. (1999). Motions, Forces And Mode Transitions In Vortex-Induced Vibrations At Low Mass-Damping. *Journal of Fluids and Structures*. 13(7-8), 813–851. ISSN 0889-9746. doi:10.1006/jfls.1999.0236.

Kim, E. S. and Bernitsas, M. M. (2016). Performance prediction of horizontal hydrokinetic energy converter using multiple-cylinder synergy in flow induced motion. *Applied Energy*. 170, 92–100. ISSN 03062619. doi:10.1016/j.apenergy.2016.02.116.

Kim, E. S., Sun, H., Park, H., chul Shin, S., Chae, E. J., Ouderkirk, R. and Bernitsas, M. M. (2021). Development of an alternating lift converter utilizing flow-induced oscillations to harness horizontal hydrokinetic energy. *Renewable and Sustainable Energy Reviews*. 145, 111094. ISSN 18790690. doi:10.1016/j.rser.2021.111094.

Kinaci, O. K., Lakka, S., Sun, H. and Bernitsas, M. M. (2016). Effect of tip-flow on vortex induced vibration of circular cylinders for Re. *Ocean Engineering*. 117, 130–142. ISSN 0029-8018. doi:10.1016/j.oceaneng.2016.03.055.

Kluger, J., Moon, F. and Rand, R. (2013). Shape optimization of a blunt body Vibro-wind galloping oscillator. *Journal of Fluids and Structures*. 40, 185–200. ISSN 0889-9746. doi:10.1016/j.jfluidstructs.2013.03.014.

Koide, M., Kato, N., Yamada, S., Kawabata, Y., Takahashi, T. and Shirakashi, M. (2007). Influence Of A Cruciform Arrangement Downstream Strip-Plate On Crossflow Vibration. *Journal of Computational and Applied Mechanics*. 8(2), 135–148.

Koide, M., Ootani, K., Yamada, S., Takahashi, T. and Shirakashi, M. (2006). Vortex Excitation Caused by Longitudinal Vortices Shedding from Cruciform Cylinder System in Water Flow. *JSME International Journal*. 49(4), 1043–1048.

Koide, M., Sekizaki, T., Yamada, S., Takahashi, T. and Shirakashi, M. (2009). A Novel Technique for Hydroelectricity Utilizing Vortex Induced Vibration. In *Proceedings of the ASME Pressure Vessels and Piping Division Conference, PVP2009-77487*. January.

Koide, M., Sekizaki, T., Yamada, S., Takahashi, T. and Shirakashi, M. (2013). Prospect of Micro Power Generation Utilizing VIV in Small Stream Based on Verification Experiments of Power Generation in Water Tunnel. *Journal of Fluid Science and Technology*. 8(3), 294–308. ISSN 1880-5558. doi:10.1299/jfst.8.294.

Koide, M., Takahashi, T., Shirakashi, M. and Salim, S. A. Z. B. S. (2017). Three-dimensional structure of longitudinal vortices shedding from cruciform two-cylinder systems with different geometries. *Journal of Visualization*, 1–11.

Krishnendu, P. and Ramakrishnan, B. (2020). Performance analysis of dual sphere wave energy converter integrated with a chambered breakwater system. *Applied Ocean Research*. 101, 102279. ISSN 0141-1187. doi:10.1016/j.apor.2020.102279.

Ledda, P. G., Siconolfi, L., Viola, F., Gallaire, F. and Camarri, S. (2018). Suppression of von Kármán vortex streets past porous rectangular cylinders. In *Physical Review Fluids*, vol. 3. October. American Physical Society. ISSN 2469-990X, 103901. doi:10.1103/PhysRevFluids.3.103901.

Li, S., Li, S., Laima, S. and Li, H. (2021). Data-driven modeling of bridge buffeting in the time domain using long short-term memory network based on structural health monitoring. *Structural Control and Health Monitoring*, e2772. ISSN 1545-2255. doi:10.1002/stc.2772.

Lin, L. M., Zhong, X. F. and Wu, Y. X. (2018). Effect of perforation on flow past a conic cylinder at Re = 100: vortex-shedding pattern and force history. *Acta Mechanica Sinica/Lixue Xuebao*. 34(2), 238–256. ISSN 1614-3116. doi: 10.1007/s10409-017-0707-2.

Liu, G., Li, H., Qiu, Z., Leng, D., Li, Z. and Li, W. (2020). *A mini review of recent progress on vortex-induced vibrations of marine risers*. doi:10.1016/j.oceaneng. 2019.106704.

Liu, H., Qu, Y., Xie, F. and Meng, G. (2022). Vortex-induced vibration of large deformable underwater composite beams based on a nonlinear higher-order shear deformation zig-zag theory. *Ocean Engineering*. 250, 111000. ISSN 0029-8018. doi:10.1016/J.OCEANENG.2022.111000.

Ma, C., Sun, H. and Bernitsas, M. M. (2018). Nonlinear piecewise restoring force in hydrokinetic power conversion using flow-induced vibrations of two tandem

cylinders. *Journal of Offshore Mechanics and Arctic Engineering*. 140(4). doi: 10.1115/1.4038584.

Ma, C., Sun, H., Nowakowski, G., Mauer, E. and Bernitsas, M. M. (2016). Nonlinear piecewise restoring force in hydrokinetic power conversion using flow induced motions of single cylinder. *Ocean Engineering*. ISSN 0029-8018. doi: 10.1016/j.oceaneng.2016.10.020.

Maruai, N. M. (2019). *Micro Energy Harvesting Using a Square Cylinder with Downstream Flat Plate*. Ph.D. Thesis. Universiti Teknologi Malaysia.

Maruai, N. M., Ali, M. S. M., Ismail, M. H. and Zaki, S. A. (2018). Flow-induced vibration of a square cylinder and downstream flat plate associated with micro-scale energy harvester. *Journal of Wind Engineering and Industrial Aerodynamics*. 175, 264–282. doi:10.1016/j.jweia.2018.01.010.

Maruai, N. M., Mat Ali, M. S., Ismail, M. H. and Shaikh Salim, S. A. Z. (2017). Downstream flat plate as the flow-induced vibration enhancer for energy harvesting. *Journal of Vibration and Control*, 107754631770787. ISSN 1077-5463. doi:10. 1177/1077546317707877.

Mat Ali, M. S., Doolan, C. J. and Wheatley, V. (2011). Low Reynolds number flow over a square cylinder with a splitter plate. *Physics of Fluids*. 23(3). ISSN 1070-6631. doi:10.1063/1.3563619.

Mat Ali, M. S., Doolan, C. J. and Wheatley, V. (2012). Low Reynolds number flow over a square cylinder with a detached flat plate. *International Journal of Heat and Fluid Flow*. 36, 133–141. ISSN 0142-727X. doi:10.1016/j.ijheatfluidflow.2012.03.011.

Mehdipour, I., Madaro, F., Rizzi, F. and Vittorio, M. D. (2022). Comprehensive experimental study on bluff body shapes for vortex-induced vibration piezoelectric energy harvesting mechanisms. *Energy Conversion and Management: X*. 13, 100174. ISSN 2590-1745. doi:10.1016/J.ECMX.2021.100174.

Mei, Y. F., Zheng, C., Aubry, N., Li, M. G., Wu, W. T. and Liu, X. (2021). Active control for enhancing vortex induced vibration of a circular cylinder based on deep reinforcement learning. *Physics of Fluids*. 33(10), 103604. ISSN 1070-6631. doi: 10.1063/5.0063988. Retrievable at `https://aip.scitation.org/doi/abs/10.1063/5.0063988`.

Meng, S., Chen, Y. and Che, C. (2020). Slug flow's intermittent feature affects VIV responses of flexible marine risers. *Ocean Engineering*. ISSN 0029-8018. doi: 10.1016/j.oceaneng.2019.106883.

Mohamed, A., Zaki, S. A., Shirakashi, M., Mat Ali, M. S. and Samsudin, M. Z. (2021). Experimental investigation on vortex-induced vibration and galloping of rectangular cylinders of varying side ratios with a downstream square plate. *Journal of Wind Engineering and Industrial Aerodynamics*. 211, 104563. ISSN 01676105. doi:10.1016/j.jweia.2021.104563.

Nakamura, T., Kaneko, S., Fumio, I., Minoru, K., Kunihiko, I., Nishihara, T., Mureithi, N. W. and Mikael A., L. (2013). *Flow-Induced Vibrations: Classifications and Lessons from Practical Experiences*. Butterworth-Heinemann. ISBN 0080983529. Retrievable at `https://books.google.com/books?hl=en{&}lr={&}id=LQusIJlDbswC{&}pgis=1`.

Nguyen, T., Koide, M., Takahashi, T. and Shirakashi, M. (2010). Universality of longitudinal vortices shedding from a cruciform two circular cylinder system in uniform flow. *Journal of Fluid Science and Technology*. 5(3), 603–616.

Nguyen, T., Koide, M., Yamada, S., Takahashi, T. and Shirakashi, M. (2012). Influence of mass and damping ratios on VIVs of a cylinder with a downstream counterpart in cruciform arrangement. *Journal of Fluids and Structures*. 28, 40–55. ISSN 0889-9746. doi:10.1016/j.jfluidstructs.2011.10.006.

Park, H., Ajith Kumar, R. and Bernitsas, M. M. (2016). Suppression of vortex-induced vibrations of rigid circular cylinder on springs by localized surface roughness at $3 \times 10^4 \leq \mathrm{Re} \leq 1.2 \times 10^5$. *Ocean Engineering*. 111, 218–233. ISSN 0029-8018. doi:10.1016/j.oceaneng.2015.10.044.

Park, H., Kim, E. S. and Bernitsas, M. M. (2017). Sensitivity to Zone Covering of the Map of Passive Turbulence Control to Flow-Induced Motions for a Circular Cylinder at $30000 \leq \mathrm{Re} \leq 120000$. *Journal of Offshore Mechanics and Arctic Engineering*. 139(2), 021802. ISSN 0892-7219. doi: 10.1115/1.4035140. Retrievable at `https://asmedigitalcollection.asme.org/offshoremechanics/article/doi/10.1115/1.4035140/377160/Sensitivity-to-Zone-Covering-of-the-Map-of-Passive`.

Park, H., Kumar, R. A. and Bernitsas, M. M. (2013). Enhancement of flow-induced motion of rigid circular cylinder on springs by localized surface roughness at $3\times10^4 \leq Re \leq 1.2 \times 10^5$. *Ocean Engineering*. 72, 403–415. ISSN 0029-8018. doi:10.1016/j.oceaneng.2013.06.026.

Raghavan, K. (2007). *Energy Extraction from a Steady Flow Using Vortex Induced Vibration.* Doctoral dissertation. The University of Michigan.

Rahman, M. R., Hasan, A. B. and Labib, M. I. (2015). Numerical investigation of aerodynamic hysteresis for transonic flow over a supercritical airfoil. In *Procedia Engineering*, vol. 105. jan. Elsevier Ltd. ISSN 18777058, 368–374. doi:10.1016/j.proeng.2015.05.021.

Rai, M. M. (2018). Vortex shedding characteristics of the wake of a thin flat plate with a circular trailing edge. *International Journal of Heat and Fluid Flow*. 72, 20–36. ISSN 0142-727X. doi:10.1016/j.ijheatfluidflow.2018.05.015.

Richardson, L. F. and Gaunt, J. A. (1927). The deferred approach to the limit. *Philosophical Transactions of the Royal Society A*. ISSN 1364-5021. doi:10.1098/rsta.1927.0008.

Saint-Michel, B., Dubrulle, B., Marié, L., Ravelet, F. and Daviaud, F. (2014). Influence of Reynolds number and forcing type in a turbulent von Kármán flow. *New Journal of Physics*. 16(6), 063037. ISSN 13672630. doi:10.1088/1367-2630/16/6/063037.

Sakamoto, K., Hemsuwan, W. and Takahashi, T. (2021). Development of a wind turbine driven by longitudinal vortex: Wind tunnel experiment to investigate the basic characteristics of the wind turbine using a single circular cylinder blade. *Journal of Wind Engineering and Industrial Aerodynamics*. 210, 104492. ISSN 01676105. doi:10.1016/j.jweia.2020.104492.

Shao, W. D. and Li, J. (2016). Numerical prediction of noise induced by flow around a cylinder considering the convection effect. *Kung Cheng Je Wu Li Hsueh Pao/Journal of Engineering Thermophysics*. ISSN 0253-231X.

Shirakashi, M., Mizuguchi, K. and Bae, H. M. (1989). Flow-induced excitation of an elastically-supported cylinder caused by another located downstream in cruciform arrangement. *Journal of Fluids and Structures*. 3(6), 595–607. ISSN 1095-8622. doi:10.1016/S0889-9746(89)90150-3.

Shirakashi, M., Takahashi, T., Kumagai, I. and Matsumoto, T. (2001). Vortex-induced vibration of the upstream cylinder of a two-cylinder system in cruciform arrangement. *Journal of Computational and Applied Mechanics*. 2(1), 103–122.

Sinha, A. (2010). *Vibration of Mechanical Systems*. Cambridge University Press.

Spalart, P. and Allmaras, S. (1992). A one-equation turbulence model for aerodynamic flows. In *30th Aerospace Sciences Meeting and Exhibit*. January. ISBN 0034-1223. ISSN 0034-1223. doi:10.2514/6.1992-439.

Stern, F., Wilson, R. V., Coleman, H. W. and Paterson, E. G. (2001). Comprehensive approach to verification and validation of CFD simulations part 1: methodology and procedures. *Journal of fluids engineering*. 123(4), 793–802.

Sun, H., Kim, E. S., Nowakowski, G., Mauer, E. and Bernitsas, M. M. (2016). Effect of mass-ratio, damping, and stiffness on optimal hydrokinetic energy conversion of a single, rough cylinder in flow induced motions. *Renewable Energy*. 99, 936–959. ISSN 0960-1481. doi:10.1016/j.renene.2016.07.024.

Sun, H., Ma, C. and Bernitsas, M. M. (2018). Hydrokinetic power conversion using Flow Induced Vibrations with nonlinear (adaptive piecewise-linear) springs. *Energy*. 143, 1085–1106. ISSN 0360-5442. doi:10.1016/j.energy.2017.10.140.

Sun, H., Ma, C., Kim, E. S., Nowakowski, G., Mauer, E. and Bernitsas, M. M. (2019). Flow-induced vibration of tandem circular cylinders with selective roughness: Effect of spacing, damping and stiffness. *European Journal of Mechanics, B/Fluids*. 74, 219–241. ISSN 0997-7546. doi:10.1016/j.euromechflu.2018.10.024.

Takahashi, T., Baranyi, L. and Shirakashi, M. (1999). Configuration and Frequency of Longitudinal Vortices Shedding from Circular Cylinders in Cruciform Arrangement. *Journal of the Visualization Society of Japan*. 19(75), 64–72. doi:10.3154/jvs.19.75_328.

Tang, M. F., Dong, G. H., Xu, T. J., wei Bi, C. and Wang, S. (2021). Large-eddy simulations of flow past cruciform circular cylinders in subcritical Reynolds numbers. *Ocean Engineering*. 220, 108484. ISSN 00298018. doi:10.1016/j.oceaneng.2020.108484.

Thompson, M., Hourigan, K. and Sheridan, J. (1994). Three-dimensional instabilities in the cylinder wake. In *Proc. Int. Colloq. Jets, Wakes, Shear Layers (Melbourne, Australia, April 18-20 1994)*. April.

Wang, S., Wen, F., Shi, X. and Zhou, X. (2019). Stability analysis of asymmetric wakes. *Physics of Fluids*. ISSN 1089-7666. doi:10.1063/1.5098111.

Wen, C., Wang, J., Zhang, Y., Xu, T., Zhang, X. and Ning, Y. (2020). Vehicle Trajectory Clustering and Anomaly Detection at Freeway Off-Ramp Based on Driving Behavior Similarity. In *CICTP 2020*. August. Reston, VA: American Society of Civil Engineers. ISBN 9780784482933, 4220–4232. doi:10.1061/9780784482933.362.

Williamson, C. (1996a). Vortex Dynamics in the Cylinder Wake. *Annual Review of Fluid Mechanics*. 28(1), 477–539. ISSN 0066-4189. doi:10.1146/annurev.fl.28.010196.002401.

Williamson, C. H. K. (1996b). Three-dimensional wake transition. *Journal of Fluid Mechanics*. 328(-1), 345. ISSN 0022-1120. doi:10.1017/S0022112096008750.

Wu, Z. and Huang, N. E. (2008). Ensemble Empirical Mode Decomposition: A Noise-Assisted Data Analysis Method. *Advances in Adaptive Data Analysis*. ISSN 1793-5369. doi:10.1142/s1793536909000047.

Xia, Y., Michelin, S. and Doaré, O. (2015). Fluid-solid-electric lock-in of energy-harvesting piezoelectric flags. *Physical Review Applied*. 3(1), 14009. ISSN 2331-7019. doi:10.1103/PhysRevApplied.3.014009.

Xu, W., Ji, C., Sun, H., Ding, W. and Bernitsas, M. M. (2017). Flow-induced vibration (FIV) and hydrokinetic power conversion of two staggered, low mass-ratio cylinders, with passive turbulence control in the TrSL3 flow regime ($2.5\times10^4$<Re<$1.2\times10^5$). In *Proceedings of the International Conference on Offshore Mechanics and Arctic Engineering - OMAE*, vol. 10. September. doi:10.1115/OMAE2017-62693.

Xu, W., Ji, C., Sun, H., Ding, W. and Bernitsas, M. M. (2019). Flow-induced vibration of two elastically mounted tandem cylinders in cross-flow at subcritical Reynolds numbers. *Ocean Engineering*. 173, 375–387. ISSN 0029-8018. doi:10.1016/J.OCEANENG.2019.01.016.

Yang, B., Yang, F., Liang, B., Zhang, Q., Wang, Z. and Wang, J. (2022). Numerical investigation of the interaction between the moving plate and sediment plume. *Ocean*

*Engineering*. 248, 110839. ISSN 0029-8018. doi:10.1016/J.OCEANENG.2022.110839.

Yokoi, Y. (2016). Flow visualization of the vortex shedding from an in-line oscillating circular cylinder with splitter plate. In *AIP Conference Proceedings*, vol. 1745. June. American Institute of Physics Inc. ISBN 9780735414020. ISSN 1551-7616, 020066. doi:10.1063/1.4953760.

Yuan, W., Sun, H., Li, H. and Bernitsas, M. M. (2020). Flow-induced oscillation patterns for two tandem cylinders with turbulence stimulation and variable stiffness and damping. *Ocean Engineering*. 218, 108237. ISSN 00298018. doi:10.1016/j.oceaneng.2020.108237. Retrievable at `https://linkinghub.elsevier.com/retrieve/pii/S0029801820311598`.

Zdravkovich, M. (1985). Flow induced oscillations of two interfering circular cylinders. *Journal of Sound and Vibration*. 101(4), 511–521. ISSN 0022-460X. doi:10.1016/S0022-460X(85)80068-7.

Zdravkovich, M. M. (1997). *Flow around circular cylinders*. ISBN 0198563965.

Zhang, B., Li, B., Fu, S., Ding, W. and Mao, Z. (2022a). Experimental investigation of the effect of high damping on the VIV energy converter near the free surface. *Energy*. 244, 122677. ISSN 0360-5442. doi:10.1016/J.ENERGY.2021.122677.

Zhang, B., Mao, Z., Song, B., Ding, W. and Tian, W. (2018a). Numerical investigation on effect of damping-ratio and mass-ratio on energy harnessing of a square cylinder in FIM. *Energy*. 144, 218–231. doi:10.1016/j.energy.2017.11.153.

Zhang, D., Sun, H., Wang, W. and Bernitsas, M. M. (2018b). Rigid cylinder with asymmetric roughness in Flow Induced Vibrations. *Ocean Engineering*. 150, 363–376. ISSN 0029-8018. doi:10.1016/j.oceaneng.2018.01.005.

Zhang, H., Xin, D. and Ou, J. (2016). Wake control of vortex shedding based on spanwise suction of a bridge section model using Delayed Detached Eddy Simulation. *Journal of Wind Engineering and Industrial Aerodynamics*. 155, 100–114. ISSN 0167-6105. doi:10.1016/j.jweia.2016.05.004.

Zhang, H., Xin, D. and Ou, J. (2019). Wake control using spanwise-varying vortex generators on bridge decks: A computational study. *Journal of Wind Engineering*

*and Industrial Aerodynamics*. 184, 185–197. ISSN 0167-6105. doi:10.1016/j.jweia.2018.11.031.

Zhang, J., Guo, H., Tang, Y. and Li, Y. (2020). Effect of top tension on vortex-induced vibration of deep-sea risers. *Journal of Marine Science and Engineering*. ISSN 2077-1312. doi:10.3390/jmse8020121.

Zhang, L., Meng, B., Tian, Y., Meng, X., Lin, X., He, Y., Xing, C., Dai, H. and Wang, L. (2022b). Vortex-induced vibration triboelectric nanogenerator for low speed wind energy harvesting. *Nano Energy*. 95, 107029. ISSN 2211-2855. doi:10.1016/J.NANOEN.2022.107029.

Zhao, M. and Lu, L. (2018). Numerical simulation of flow past two circular cylinders in cruciform arrangement. *Journal of Fluid Mechanics*. 848, 1013–1039. ISSN 0022-1120. doi:10.1017/jfm.2018.380.

Zou, B., Thierry, N. N. B., Tang, H., Xu, L., Zhou, C., Wang, X., Dong, S. and Hu, F. (2021). Flow field and drag characteristics of netting of cruciform structures with various sizes of knot structure using CFD models. *Applied Ocean Research*. 106, 102466. ISSN 01411187. doi:10.1016/j.apor.2020.102466.

## LIST OF PUBLICATIONS

### Journal with Impact Factor

1. **Ahmad Adzlan Fadzli Bin Khairi**, Mohamed Sukri Mat Ali, Sheikh Ahmad Zaki: *Temporal Evolution of Lift in a Pure Cruciform System for Energy Harvesting*, **Ocean Engineering** (IF:3.795, Q1) 2021. **PUBLISHED.**

### Indexed Journal (SCOPUS)

1. **Ahmad Adzlan Fadzli Bin Khairi**, Mohamed Sukri Mat Ali: *OpenFOAM Implementation for The Study of Streamwise Vortex-Induced Vibration-Based Energy Harvester for Sensor Networks*, **Journal of Advanced Research in Fluid Mechanics and Thermal Sciences** 2018. **PUBLISHED.**